THE ASTROPHYSICAL JOURNAL, 445:314–324, 1995 May 20

PROPERTIES OF THE +70 KILOMETERS PER SECOND CLOUD TOWARD HD 203664

KENNETH R. SEMBACH[1]
Center for Space Research, 6-216, Massachusetts Institute of Technology, 77 Massachusetts Avenue, Cambridge, MA 02139
Received 1994 September 6; accepted 1994 November 22

ABSTRACT

I present high-resolution *International Ultraviolet Explorer* spectra of the ultraviolet absorption in an intermediate-velocity interstellar cloud ($v_{LSR} \approx +70$ km s^{-1}) toward HD 203664. The combined, multiple *IUE* images result in spectra with S/N = 15–40 and resolutions of approximately 20–25 km s^{-1}. The intermediate-velocity cloud absorption is present in ultraviolet lines of C II, C II*, C IV, N I, O I, Mg I, Mg II, Al II, Al III, Si II, Si III, Si IV, S II, Cr II, Mn II, Fe II, and Zn II. The relative abundances of low-ionization species suggest an electron density of 0.15–0.34 cm^{-3} and a temperature of 5300–6100 K in the neutral and weakly ionized gas. Given the presence of high-ionization gas tracers such as Si IV and C IV, ionized portions of the cloud probably contribute to the relatively large values of n_e derived from measurements of the lower ionization species. The high-ionization species in the cloud have an abundance ratio, N(C IV)/N(Si IV) ≈ 4.5, similar to that inferred for collisionally ionized cloud interfaces at temperatures near 10^5 K along other sight lines. When referenced to sulfur, the abundances of most elements in the cloud are within a factor of 5 of their solar values, which suggests that the +70 km s^{-1} gas has a previous origin in the Galactic disk despite a recent determination by Little et al. that the cloud lies at a distance of 200–1500 pc below the Galactic plane. I have checked this result against a model of the ionization for the diffuse ionized gas layer of the Galaxy and find that this conclusion is essentially unchanged as long as the ionization parameter is low as implied by the abundances of adjoining ionization states of aluminum and silicon. The processes responsible for the production of highly ionized gas in the +70 km s^{-1} cloud appear to be able to account for the inferred dust grain destruction as well.

Subject headings: ISM: abundances — ISM: clouds — stars: individual (HD 203664) — ultraviolet: ISM

1. INTRODUCTION

The observational study of most intermediate- and high-velocity clouds (IVCs and HVCs) presents an interesting challenge due to their low gas column densities, small angular sizes, and lack of suitable background continuum sources. Despite recent radio surveys designed to identify HVC complexes in the Milky Way (Hulsbosch & Wakker 1988; Wakker & van Woerden 1991), little information exists about the fundamental properties of the intermediate- and high-velocity clouds (i.e., temperature, ionization structure, density, and distance). Studies using QSOs and bright Seyfert nuclei as background sources have detected many HVCs in strong lines of low-ionization metals such as Fe II and Mg II and, in a few cases, higher ionization lines of C IV (Savage et al. 1993a). The crude abundance estimates and velocity information that result from the low resolution of these studies can often be improved upon by higher resolution data (e.g., Bowen & Blades 1993; Savage et al. 1993b; Lu, Savage, & Sembach 1994; Savage, Sembach, & Lu 1995), but the observing time required permits detailed studies of only a few species, and meaningful distance determinations for the intermediate- and high-velocity gas features are usually not possible due to the "infinite" path of the sight line. Both optical and ultraviolet studies of bright halo stars at large distances from the Galactic plane have also provided crude information on the abundances in HVCs (Keenan et al. 1983; Danly, Albert, & Kuntz 1993; Sembach, Savage, & Lu 1995).

In this paper I present new high-resolution *International Ultraviolet Explorer* (*IUE*) measurements of the interstellar gas distribution toward HD 203664 ($l = 61.^\circ9$, $b = -27.^\circ5$, $d = 3.2$ kpc, $z = -1.5$ kpc). This sight line contains an intermediate velocity cloud at $v_{LSR} \approx +70$ km s^{-1} that has been studied recently by both Albert et al. (1993) and Little et al. (1994) at optical and radio wavelengths.[2] Their absorption-line measurements show that the +70 km s^{-1} cloud must lie at a z-distance between $\approx$200 and 1500 pc, and new optical data being collected while this work is in progress will further constrain the location of the cloud.

The HD 203664 +70 km s^{-1} cloud was studied previously with the *IUE* by Bates et al. (1983) as part of a search for high-velocity gas in the general direction of the Loop II supernova remnant ($l \approx 100^\circ$, $b \approx -32^\circ$, diameter $\approx 91^\circ$; Berkuijsen, Haslam, & Salter 1971). The new data obtained for the present study expand upon this previous analysis by quantitatively assessing the range of allowed abundances and conditions in the cloud, reporting new detections of ionized gas species (Al III, Si IV, C IV), and making rough estimates of several singly ionized gas species (Mn II, Cr II, Zn II) that were not detected toward this cloud before.

[1] Hubble Fellow and Guest Observer with the *International Ultraviolet Explorer* Satellite, sponsored and operated by the National Aeronautics and Space Administration (USA), the Science and Engineering Research Council (UK), and the European Space Agency.

[2] I have adopted the term "intermediate-velocity" when referring to the HD 203664 +70 km s^{-1} absorption to distinguish between the velocities of this cloud(s) and those of the "high-velocity" cloud system in the Galaxy. This distinction is still somewhat poorly defined at present, and the definition depends to some extent upon individual preferences. Recently, Danly (1989) and Danly et al. (1992) have defined $|v| > 70$ km s^{-1} as "high-velocity", whereas Hulsbosch & Wakker (1988) used $|v| > 100$ km s^{-1} as the cutoff. By either definition, the HD 203664 cloud is more properly classified as an IVC than as an HVC and, since Galactic rotation may account for some (up to $\approx$25 km s^{-1}) of the velocity of the cloud if it is located at a large distance along the sight line, I choose the former classification.

This paper is organized as follows: In § 2 I describe the observations and data reduction procedures for the study. Section 3 is a discussion of the methods used to determine line strengths and column densities, and § 4 contains comments on the absorption seen in each species. Sections 5 and 6 provide information about the physical conditions and abundances within the cloud. A short discussion and summary of the primary results of the paper are provided in § 7.

2. OBSERVATIONS AND REDUCTIONS

In 1994 June I obtained four SWP (1150–2000 Å) and three LWP (2000–3200 Å) high-dispersion echelle spectra under *IUE* program GHQKS to study the intermediate velocity absorption toward HD 203664. For each exposure, I offset the star in the large aperture to change the fixed pattern noise structure in the extracted spectrum, and I overexposed several of the images at the long-wavelength portions of the detectors to increase the signal-to-noise ratios for shorter wavelength regions. When these images were combined with several available for each camera from the *IUE* data archives, a composite spectrum for each wavelength range with a resolution of 20 to 25 km s^{-1} resulted (see Sembach & Savage 1992 for a discussion of this procedure). Table 1 gives a summary of the exposure times, aperture locations, and heliocentric velocity offsets for each of the images. For the combined SWP spectrum, S/N $\approx$ 15–40 depending upon the stellar flux level and detector sensitivity as a function of wavelength. For the combined LWP spectrum, S/N $\approx$ 15–25.

SWP 37035 and LWP 16369 served as the velocity templates for the remaining images. Comparison of the strong Si II lines present in the SWP 37035 spectrum with the strong Fe II lines in the LWP 16369 spectrum indicated that there is no significant velocity offset between the combined short- and long-wavelength spectra. The absolute heliocentric velocities provided by the standard *IUE* processing should be accurate to within 10 km s^{-1} based upon the shifts determined for other images obtained with the starlight centered in the large aperture. All velocities quoted in this paper are referenced to the local standard of rest (LSR), where $v_{LSR} = v_{helio} + 9.9$ km s^{-1}.

Application of a secondary background correction for wavelengths shortward of 1350 Å was necessary to compensate for the inadequate background subtraction provided by the standard processing and the primary reduction procedures. The corrections consisted of linear increases or decreases to the net intensities of the lines determined from the zero levels of the cores of strongly saturated lines at these wavelengths. For any given line, this correction was less than 6% of the continuum level, and in most cases the correction was only 2%–3%. The residual background uncertainty present in the data at short wavelengths after this correction is probably less than 2%.

TABLE 1

HD 203664 *IUE* HIGH-DISPERSION SPECTRA

Image	Exposure Time (minutes)	Aperture Location	V_{shift} (km s^{-1})	Note
SWP 07354.....	30	Center	−13	1
SWP 07355.....	36	Center	−12	1
SWP 10069.....	30	Center	−3	1
SWP 37035.....	45	Center	0	1, 2
SWP 37036.....	65	Center	+5	1, 3
SWP 51083.....	70	Offset	−23	3, 4
SWP 51084.....	70	Offset	+31	3, 4
SWP 51085.....	65	Offset	−15	3, 4
SWP 51086.....	50	Offset	+14	4
LWP 16368.....	30	Center	−12	1
LWP 16369.....	30	Center	0	1, 2
LWP 28408.....	30	Offset	+27	4
LWP 28409.....	30	Offset	−27	4
LWP 28410.....	42	Offset	+12	3, 4

NOTES.—(1) Image from *IUE* data archives. (2) Image used as heliocentric velocity template ($v_{LSR} = v_{helio} + 10$ km s^{-1}). (3) Image overexposed to increase detectability of weak features. (4) Image obtained in 1994 June.

Some of the ultraviolet interstellar absorption lines toward HD 203664 are illustrated in Figure 1, where the profiles have been normalized to a unity continuum level by dividing the observed intensity levels by a continuum estimated from a low-order (≤ 5) polynomial fit to regions of the spectrum within ± 300 km s^{-1} of each line. A complete description of the continuum fitting process is given by Sembach & Savage (1992). The large projected rotational velocity of HD 203664 ($v \sin i \approx 200$ km s^{-1}; Lennon et al. 1991) makes continuum placement unambiguous for all of the illustrated interstellar lines, except as noted in Table 2. Several examples of unnormalized interstellar profiles are displayed in Figure 2 along with a photospheric Si III* line, which was used to judge the approximate behavior of the stellar continuum at velocities covered by the interstellar lines.

The HD 203664 sight line has been observed by Little et al. (1994) at 21 cm wavelengths with a 12′ × 12′ beam and a velocity resolution of 3.5 km s^{-1}. The H I radio data are shown at the top left of Figure 1 with brightness temperature (in K) plotted versus LSR velocity. The radio data clearly show 21 cm emission at velocities corresponding to the +70 km s^{-1} absorption in the ultraviolet lines observed with the *IUE*.

3. MEASUREMENTS

Table 2 contains equivalent widths and apparent column densities for 43 absorption lines between 1190 and 2860 Å. The usual definition for an *apparent* column density in units of (ions cm^{-2} [km s^{-1}]$^{-1}$) is

$$N_a = \int N_a(v)dv = \frac{m_e c/\pi e^2}{f\lambda} \int \tau_a(v)dv$$

$$= 3.768 \times 10^{14} \int \frac{\ln[-I(v)]}{f\lambda}\, dv\,, \qquad (1)$$

where $\tau_a(v)$ is the *apparent* optical depth profile, $I(v)$ is the continuum normalized absorption profile, f is the oscillator strength of the line, and λ is the wavelength in Å. The wavelengths and f-values of each line are from the atomic data compilation given by Morton (1991) unless otherwise indicated in § 4 or in the notes following Table 2. The integration in equation (1) extends over all velocities, but for practical reasons only the range from $\approx +50$ km s^{-1} to $\approx +110$ km s^{-1} is used to isolate the higher velocity results from the main velocity absorption at smaller velocities and excess noise contributions at larger velocities. This velocity range spans the intermediate-velocity Ca II absorption components observed toward HD 203664 (Albert et al. 1993; Keenan et al. 1983; Little et al. 1994). The apparent column density described by the above equation is indistinguishable from the true column density in the limits where the line is fully resolved or weak. With the possible exception of the highly ionized gas lines, none of the lines listed in Table 1 is fully resolved at the

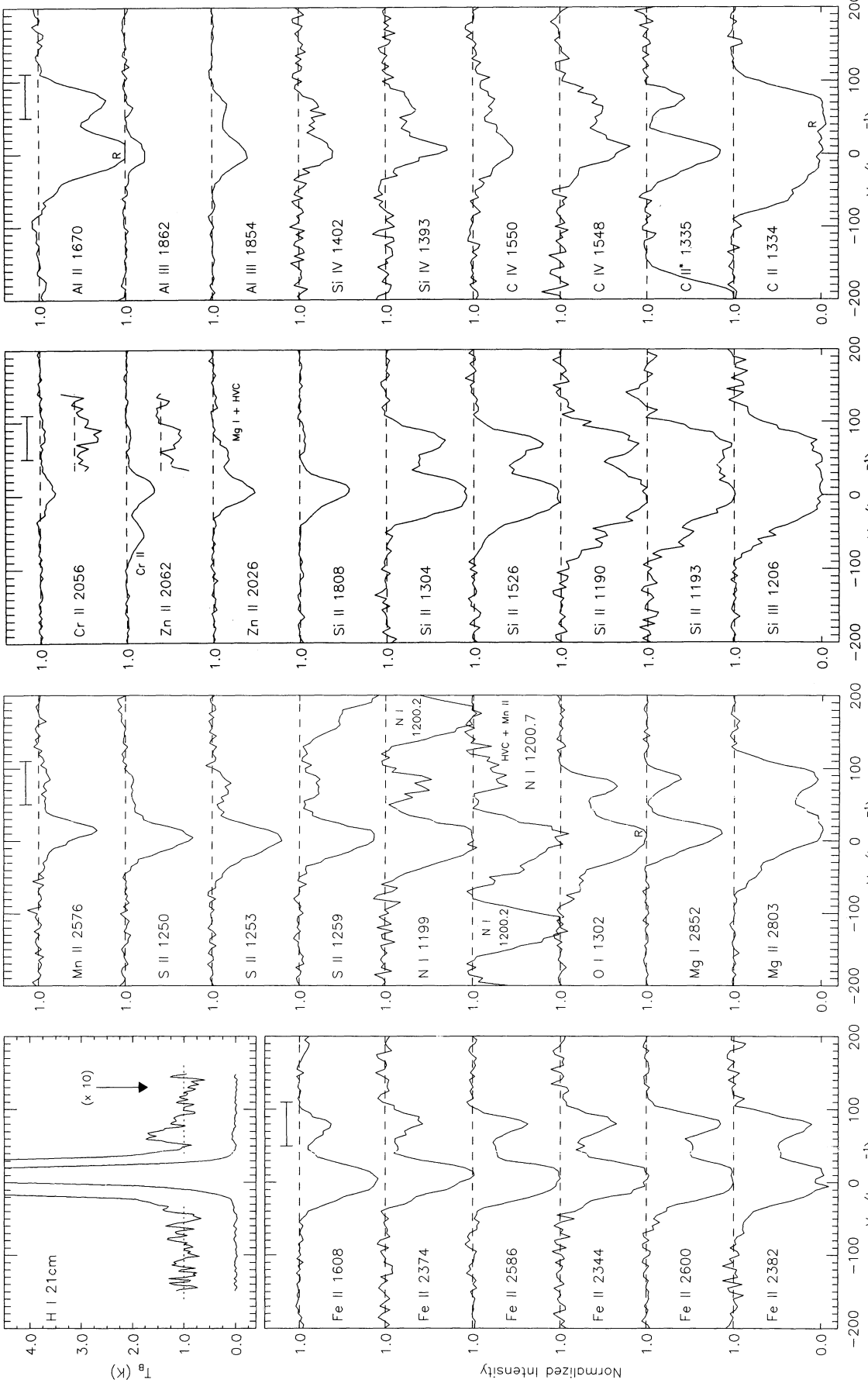

FIG. 1.—Normalized intensity vs. LSR velocity for some of the ultraviolet absorption lines exhibiting high velocity absorption near +70 km s^{-1} toward HD 203664. The spectra shown are velocity-registered combinations of multiple high-dispersion *IUE* SWP and LWP spectra obtained at various aperture offset locations (see Table 1). The spectra have S/N ≈ 15–40 depending upon wavelength of the transition and resolutions of 20–25 km s^{-1} (FWHM). All profiles have been normalized by dividing the observed intensity by a continuum fit to regions on either side of each line as discussed in § 2. For the weak lines of Cr II λ2056 and Zn II λ2062, the higher velocity absorption has been expanded by a factor of 5 and inset below the unexpanded profile. The H I 21 cm emission profile shown at the top of the first panel is from Little et al. (1994) and has a velocity resolution of 3.5 km s^{-1}.

TABLE 2

EQUIVALENT WIDTHS AND COLUMN DENSITIES OF THE +70 KILOMETERS PER SECOND CLOUD

Ion (1)	λ_{vac} (Å) (2)	f-Value[a] (3)	$W_\lambda \pm 1\ \sigma$ (mÅ) (4)	$[-1\ \sigma$ (5)	log N_a (6)	$+1\ \sigma]$ (7)	log N (8)	Method[b] (9)
C II	1334.532	1.278 (−1)	206.1 ± 8.6	...	...	...	>14.00	1
C II*	1335.708	1.149 (−1)	50.4 ± 8.3	...	>13.54	...	>13.54	2
C IV	1550.770	9.522 (−2)	48.9 ± 11.7	13.33	13.47	13.57	$13.49^{+0.06}_{-0.07}$	3
	1548.195	1.908 (−1)	99.2 ± 10.5	13.44	13.50	13.55		
N I	1199.550	1.328 (−1)	60.7 ± 8.9	...	>13.66	...	>13.66	2
	1200.223[c]	8.849 (−2)	...	...	...	...		
	1200.710[d]	4.423 (−2)	<61	...	...	...		
N V	1238.821	1.570 (−1)	<18	...	<12.93	...	<12.93	4
O I	1302.168	4.887 (−2)	96.2 ± 5.8	...	>14.24	...	>14.24	2
Mg I	2026.477	1.154 (−1)	<12	...	<12.46	...	11.92–12.46	2
	2852.964	1.830 (0)	93.3 ± 6.1	...	>11.92	...		
Mg II.....	1239.925	1.250 (−3)	<13	...	<14.88	...		5
	2803.531	3.054 (−1)	445.3 ± 6.2	13.66	13.68	13.70	$14.30^{+0.02}_{-0.08}$	
	2796.352	6.123 (−1)	477.7 ± 7.9	13.43	13.48	13.53		
Al II	1670.787	1.833 (0)	159.3 ± 6.5	...	>12.83	...	>12.83	2
Al III	1862.790	2.789 (−1)	9.0 ± 6.4	11.41	12.03	12.27	$12.30^{+0.06}_{-0.07}$	4
	1854.716	5.602 (−1)	31.5 ± 4.5	12.23	12.30	12.36		
Si II.....	1808.013[e]	2.000 (−3)	12.7 ± 4.0	14.11	14.36	14.51	$14.13^{+0.06}_{-0.06}$	5
	1304.370[f]	9.345 (−2)	110.5 ± 6.1	14.03	14.06	14.08		
	1526.707[f]	1.155 (−1)	129.9 ± 5.3	13.96	13.99	14.01		
	1190.416	2.502 (−1)	146.2 ± 6.4	13.87	13.92	13.96		
	1193.290	4.991 (−1)	161.2 ± 8.5	13.64	13.79	13.90		
Si III	1206.500	1.669 (0)	185.5 ± 9.2	...	>13.32	...	>13.32	2
Si IV	1402.770	2.553 (−1)	24.4 ± 11.0	12.57	12.84	13.00	$12.85^{+0.10}_{-0.14}$	3
	1393.755	5.140 (−1)	54.4 ± 14.8	12.70	12.86	12.97		
S II	1250.584	5.453 (−3)	14.3 ± 3.8	14.12	14.28	14.39	$14.28^{+0.07}_{-0.08}$	3
	1253.811	1.088 (−2)	27.4 ± 3.5	14.18	14.27	14.34		
	1259.519	1.624 (−2)	37.5 ± 4.2	14.19	14.27	14.34		
Cr II	2066.161	7.066 (−2)	<6:	...	<12.35:	...	$12.38^{+0.15}_{-0.08}$	6
	2062.234[g]	1.062 (−1)	...	...	...	...		
	2056.254[h]	1.420 (−1)	11.7 ± 3.1:	12.23:	12.38:	12.49:		
Mn II.....	2606.462[h]	1.927 (−1)	<14	...	<11.94	...	$12.14^{+0.16}_{-0.24}$	4
	2594.499[h]	2.710 (−1)	<19	...	<12.21	...		
	2576.877[h]	3.508 (−1)	29.4 ± 12.6	11.90	12.14	12.30		
Fe II.....	2260.780	3.715 (−3)	<24	...	<14.16	...	$13.95^{+0.05}_{-0.06}$	5
	1608.451[i]	6.194 (−2)	60.3 ± 5.4	13.68	13.72	13.76		
	2374.461	2.812 (−2)	109.6 ± 19.1	13.88	13.97	14.05		
	2586.650	6.457 (−2)	164.7 ± 8.6	13.73	13.76	13.78		
	2344.214	1.097 (−1)	175.2 ± 19.5	13.59	13.66	13.71		
	2600.173	2.239 (−1)	249.7 ± 6.6	13.52	13.54	13.56		
	2382.765	3.006 (−1)	249.9 ± 13.0	13.46	13.51	13.55		
Zn II	2062.664[h]	2.562 (−1)	7.6 ± 3.0:	11.70	11.94:	12.09:	$11.94^{+0.15}_{-0.24}$	6
	2026.136[j]	4.890 (−1)	...	...	...	...		

[a] Unless otherwise indicated, vacuum wavelengths and f-values are from the atomic data compilation given by Morton 1991.

[b] Method of calculating log N—(1) Strong absorption, no integration possible—column density limit from listed equivalent width. (2) Strong absorption—column density limit from single-line, direct integration results ($W_\lambda > 50$ mÅ). (3) Column density from average of direct integration results. (4) Column density from single-line, direct integration results ($W_\lambda < 50$ mÅ). (5) Column density from single-component curve of growth to listed values of W_λ (≥ 2 lines). (6) Column density from single-line, direct integration results ($W_\lambda < 20$ mÅ). Result may be uncertain due to noise properties of the *IUE* detectors.

[c] N I λ1200.2 +70 km s^{-1} absorption is blended with zero-velocity N I λ1200.7 absorption.

[d] N I λ1200.7 +70 km s^{-1} absorption is blended with zero-velocity Mn II λ1201.1 absorption.

[e] Oscillator strength from Dufton et al. 1982; see also Spitzer & Fitzpatrick 1993.

[f] Oscillator strength from Dufton et al. 1993; see also Cardelli et al. 1994.

[g] Cr II λ2062.2 +70 km s^{-1} absorption is blended with zero-velocity Zn II λ2062.6 absorption.

[h] Continuum placement susceptible to additional errors for this weak line.

[i] Strength of line indicates that oscillator strength may be smaller than listed value. The data in this study are better fitted if $f_{1608} \approx 0.03$ (see text). This line was omitted from the log N calculation.

[j] Zn II λ2026.1 +70 km s^{-1} absorption blended with zero-velocity Mg I λ2026.4 absorption.

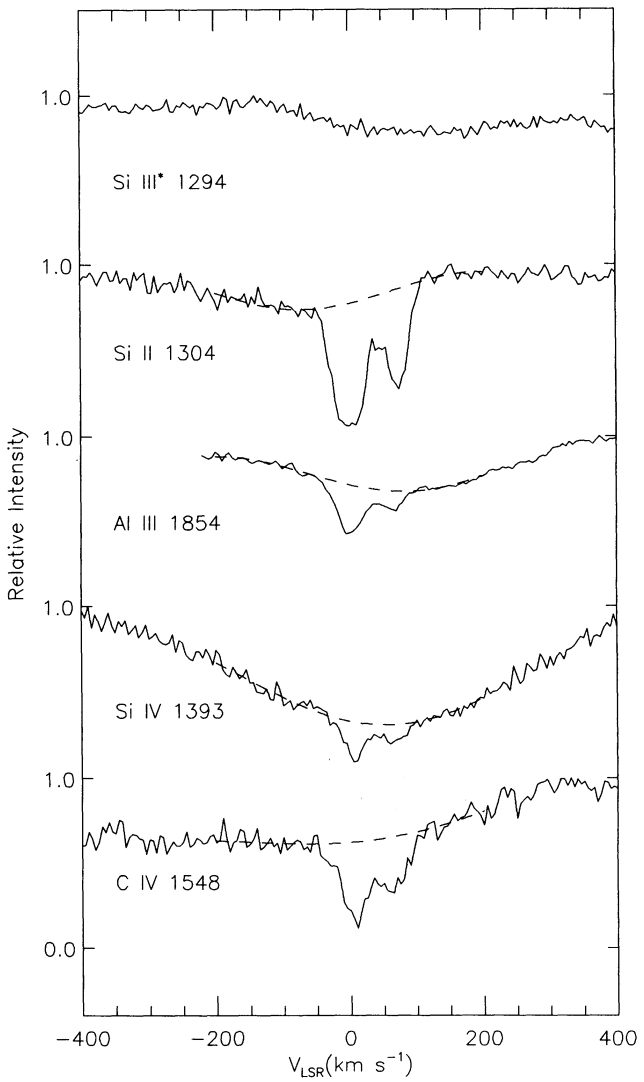

FIG. 2.—Relative intensity vs. LSR velocity for several of the normalized profiles shown in Fig. 1. The dashed lines represent the adopted continuum for each line. The stellar Si III* line shown at the top of the plot was used to help in placing the continuum levels for the interstellar lines.

20–25 km s^{-1} resolution of the data. However, several lines are weak enough ($W_\lambda \leq 20$ mÅ) to be unaffected by unresolved saturated structures, and integration of the apparent column density profile provides a reliable estimate of N. In the remaining cases the values of N_a provide strict lower limits to N. A general discussion of apparent column densities and the circumstances under which they are useful has been given by Savage & Sembach (1991).

The adopted column density for each species is listed in column (8) of Table 2. For those species with multiple lines having well-determined equivalent widths, I estimated column densities from a single-component Doppler-broadened curve of growth (COG) applied to the listed values of W_λ. This procedure provides a reliable column density estimate unless the distribution in the widths of the absorbing components contributing to the values of W_λ is unusual (e.g., a bimodal distribution with half of the components fully resolved and half completely unresolved—see Nachman & Hobbs 1973; Jenkins 1986; Savage & Sembach 1991). The optical data obtained by Little et al. (1994) indicates that the +70 km s^{-1} cloud probably has at least two components separated in velocity by approximately 10 km s^{-1}, and the component width distribution appears to be simple enough to allow accurate column density estimates using a COG. The b-values derived from the COG are probably not meaningful in absolute terms, but the similarity of the values for Mg II, Si II, S II, and Fe II ($b \approx 8$–12 km s^{-1}) suggests that these species trace similar gas distributions.

When only a single line of a species was detectable, I estimated the column density (or column density limit) from the listed apparent column density. Column (9) of Table 2 indicates the method used in computing the column density. Further details for individual species are given in § 4.

All errors on W_λ, N_a, and N in Table 2 are 1 σ estimates derived from continuum placement uncertainties and statistical noise fluctuations in the lines (see Sembach & Savage 1992, their Appendix A). Background uncertainties may also be important in some cases. A 2% background error contributes an error of approximately 0.01 dex in the logarithmic column density estimates and $0.02W_\lambda$ in the equivalent width estimates. Upper and lower limits on quantities in Table 2 are 2 σ estimates.

4. IVC ABSORPTION OVERVIEW

4.1. H I *and* S II

The S II $\lambda\lambda$1199, 1200.2, 1200.7 multiplet shows weak absorption at the velocities of the IVC. The lines span a factor of 3 difference in log $f\lambda$ and all three lines lie on the linear part of the COG as indicated by the good agreement between the integrated apparent column densities of the lines. Assuming that S is undepleted (Jenkins 1987) and a cosmic value of S/H = 1.86×10^{-5} (Anders & Grevesse 1989), the S II column density of log N(S II) = 14.28 implies an H I column density of log N(H I) = 19.01, or nearly a factor of 5 larger than the value of log N(H I) = 18.34 measured from the H I 21 cm emission profile shown in Figure 1 in the optically thin limit (Little et al. 1994). The assumption that the gas is optically thin is reasonable since the maximum brightness temperature in the cloud is less than 0.1 K.

The Na I–H I relation for low-density sight lines derived by Diplas & Sembach (1995), log N(H I) $\approx$ log N(Na I) + 8.16, yields log N(H I) $\approx$ 19.38. This neutral hydrogen column density estimate is a factor of 2.3 higher than N(H I) inferred from the S II measurements, and while this modest difference could easily be accounted for by the large scatter in the empirical Na I–H I relationship, the difference between $N(\mathrm{H\ I})_{21\ \mathrm{cm}}$ and $N(\mathrm{H\ I})_{\mathrm{Na\ I,S\ II}}$ cannot be so simply dismissed. I will show below that the H II content of the cloud may account for this difference only if the radiation field is very dilute, although even this interpretation may have difficulty in explaining the general agreement in the Na I and S II results since their ionization potentials are so different.

It is very unlikely that a significant amount of H_2 is present in the HD 203664 IVC since N(H I)/$N(H_2) > 1$ for unreddened and moderately reddened sight lines with column densities of $\sim 10^{19}$ cm^{-2} (Jenkins, Savage, & Spitzer 1986). The most likely explanation for the H I column density discrepancies is that small-scale cloud structure with angular size significantly less than the 12′ × 12′ beam used for the 21 cm emission observations hides much of the "missing" H I in the IVC (see also Albert et al. 1993). Small scale structures with sizes of 1′ are common in IVCs and HVCs (Wakker & Schwarz 1991), and

therefore further 21 cm mapping of the cloud at high resolution is desirable.

4.2. O I *and* N I

O I and N I are perhaps the best neutral gas tracers in the UV spectrum because their ionization potentials of 13.6 and 14.1 eV ensure that they are found primarily in H I regions. Unfortunately, the N I λ1200.2 and λ1200.7 IVC lines are blended with lower velocity absorption features, and the N I λ1199 and O I λ1302 lines appear to be heavily saturated (see Table 2). O and N tend to remain mostly in gaseous form in the ISM (Jenkins 1987), and therefore application of curves of growth derived for heavier elements that are often depleted onto dust grains can lead to significant column density errors. For these reasons, only the (poorly constrained) column density limits of log N(O I) > 14.24 and log N(N I) > 13.66 can be derived. The nondetection of the very weak line of O I λ1355 yields log N(O I) < 17.5.

Under the assumption that a single-component Doppler-broadened curve of growth applies, the O I and N I b-values required to produce the observed H I column density for a gas of solar composition are less than 5 km s^{-1}. It is interesting to note that Little et al. (1994) find b-values of approximately 3 km s^{-1} for the absorption by Na I and Ca II.

4.3. C II, C II*, *and* C IV

The IVC contains C II* λ1335 absorption, which is important because it arises out of a fine-structure level populated primarily through collisional excitation by electrons. The N I data indicate that lines having equivalent widths of $\approx$50 mÅ are probably saturated, so log N(C II*) > 13.54. The C II λ1334 resonance line is strongly saturated at the velocities of the IVC absorption, which results in a lower limit of log N(C II) > 14.00. The detection of the C IV $\lambda\lambda$1548, 1550 doublet provides one of the few reliable column density estimates obtained for higher ionization stages in IVCs. Both C IV lines are of modest strength with a ratio of $W_\lambda(1548)/W_\lambda(1550) \approx 2$.

4.4. Mg I *and* Mg II

The Mg II $\lambda\lambda$2796, 2803 absorption in the IVC is strong and saturated. However, a curve of growth applied to the equivalent widths in Table 2 provides a fairly reliable estimate of the Mg II column density, log N(Mg II) = 14.30. The resulting b-value of 13 km s^{-1} is similar to the 8–12 km s^{-1} b-values found for Si II, S II, and Fe II. Nondetection of the weak Mg II doublet at 1240 Å provides a consistent 2 σ upper limit of log N(Mg II) < 14.88.

The Mg I λ2852 line is easily detected at the velocities of the IVC. Its strength of $\approx$93 mÅ suggests that the line is not on the linear portion of the COG. Combined with the upper limit of log N(Mg I) < 12.46 found from the weak λ2026 line, the λ2852 result of log N(Mg I) > 11.92 yields N(Mg I)/N(Mg II) = (0.42–1.4) $\times$ 10^{-2}.

4.5. Al II *and* Al III

Both the Al II λ1670 line and the Al III $\lambda\lambda$1854, 1862 doublet absorption are present in the IVC in the ratio N(Al II)/N(Al III) > 3.4. The weaker member of the Al III doublet is not reliably detected, so it is necessary to rely upon the λ1854 line for the Al III column density estimate in Table 2. Al III is not often seen in high-velocity gas in supernova remnants (Jenkins, Silk, & Wallerstein 1986), but it is seen at high velocities in the interstellar medium toward the Galactic poles (Savage & Sembach 1994).

4.6. Si II, Si III, *and* Si IV

Several ionization stages of Si are present in the IVC. For Si II, the lines observed include $\lambda\lambda$1190, 1193, 1304, 1526, and 1808. Si II λ1260 absorption associated with the IVC is very strongly saturated and is not considered further in this paper. For the $\lambda\lambda$1304, 1526, and 1808 lines, I have adopted the f-values from Dufton et al. (1983, 1992) because recent observations with the Goddard High-Resolution Spectrograph (GHRS) have indicated that they are more accurate than other estimates (see Spitzer & Fitzpatrick 1993; Cardelli et al. 1994).

The Si III line at 1206 Å is strongly saturated and only a lower limit of log N(Si III) > 12.95 can be deduced. However, the Si IV $\lambda\lambda$1393, 1402 doublet is easily detected with a doublet ratio $W_\lambda(1393)/W_\lambda(1402) \approx 2$. A value of N(Si II)/N(Si III) < 6.4 combined with the Al results presented above indicates that the ratio of singly to doubly ionized gas in the IVC is 3.4–6.4. Since Al II and Si II are the dominant forms of Al and Si in H I regions, it appears that most of the hydrogen associated with the IVC is probably neutral (but see § 6 for a discussion of these ratios in dilute, low ionization parameter H II regions). The ratio N(Si II)/N(Si IV) = 19 implies that the highly ionized gas fraction of the IVC is approximately 5%.

4.7. Fe II

Absorption by Fe II in the $\lambda\lambda$1608, 2374, 2586, 2344, 2600, and 2382 lines is present at the IVC velocities. The Fe II COG minimization is significantly worsened by including the λ1608 line in the fit. The equivalent width and f-value of 0.0619 for the λ1608 line are inconsistent with the relative strengths of the other Fe II lines. Revisions in the f-value of the λ1608 line have changed significantly over time. The observed line strength suggests $f_{1608} \approx 0.03$, or a factor of 2 lower than the Shull & Seab (1982) value adopted by Morton (1991). The column density limit of log N(Fe II) < 14.16 derived from the nondetection of the λ2260 line is consistent with the strengths of the other Fe II lines (see Table 2). The COG fit to the Fe II lines results in log N(Fe II) = 13.95.

4.8. Mn II, Zn II, *and* Cr II

The estimates of the column densities of Mn II, Zn II, and Cr II in the IVC are based upon single line estimates. The Mn II λ2576, Zn II λ2062 and Cr II λ2056 lines are marginally detected (2–3 σ), but the remaining lines are blended with other absorption features or are too weak to be detected (see Table 2 notes). The gas phase depletions derived from these estimates in § 6 fit the trends implied by other species, but these column density estimates must be considered tentative until higher quality data can be obtained.

5. PHYSICAL CONDITIONS

The wide range of ionization states observed for the +70 km s^{-1} IVC indicates that the ionization structure of the cloud is complex. The IVC exhibits detectable absorption in species ranging from Na I ($\chi_{\rm I-II}$ = 5.14 eV) to C IV ($\chi_{\rm III-IV}$ = 47.9 eV). It is unlikely that the entire range of observed species exists in the same gas since the ionization mechanisms leading to their formation are quite different. I now discuss possible ionization mechanisms and physical condition within the gas.

5.1. *Neutral and Singly Ionized Species*

Collisional ionization of the weakly ionized species in the IVC is unlikely to be important. In a gas in collisional ioniza-

TABLE 3

ELECTRON DENSITIES AND TEMPERATURES[a]

T_e (K) (1)	n_e (cm^{-3}) {Mg I, Mg II}[b] (2)	{C II*, S II}[c] (3)	{Ca II, Fe II}[d] (4)	N(Mg I)/N(Na I) (5)
100.....	**0.023–0.081**	**>0.017**	**0.006–0.023**	**7.7**
500.....	0.092–0.319	>0.038	0.018–0.067	5.8
1000.....	0.166–0.577	>0.054	0.028–0.104	5.1
2000.....	0.301–1.043	>0.076	0.044–0.163	4.6
3000.....	0.425–1.474	>0.094	0.057–0.212	4.3
4000.....	0.512–1.774	>0.108	0.069–0.255	4.3
4500.....	0.484–1.678	>0.115	0.074–0.276	4.9
5000.....	0.386–1.339	>0.121	0.079–0.295	6.6
5500.....	**0.267–0.925**	**>0.127**	**0.085–0.314**	**10.3**
6000.....	**0.174–0.602**	**>0.133**	**0.089–0.332**	**16.7**
6500.....	0.113–0.392	>0.138	0.094–0.350	27.1
7000.....	0.077–0.265	>0.143	0.099–0.367	42.2
8000.....	0.040–0.137	>0.153	0.108–0.400	89.4

[a] Boldface values indicate acceptable agreement between the various derived quantities.

[b] Electron density range derived from Mg I and Mg II using eq. (2).

[c] Electron density limit derived from C II* and S II using eq. (3) and assuming $\delta(C) = \delta(S) = 1.0$.

[d] Electron density range derived from Ca II and Fe II using eq. (4) and assuming $\delta(Ca) = (0.0–0.33)\,\delta(Fe)$.

tion equilibrium, the relative abundances of the Mg, Al, and Si ions found in § 4 can be satisified for $T = (1.7–2.5) \times 10^4$ K (see Sutherland & Dopita 1993), but the presence of N I, O I and, Na I suggests that the gas is much cooler ($T < 10^4$ K) and contains a substantial amount of neutral material. The equilibrium ionization balance equation for photon ionizations is given by

$$n(X^{i+1}) n_e \alpha(X^i) = \Gamma(X^i) n(X^i) \quad (2)$$

where $\alpha = \alpha_{rad} + \alpha_{di}$ is the total recombination coefficient due to radiative and dielectronic recombinations and Γ is the ionization rate due to an assumed radiation field. Throughout I rely upon the standard supposition that the two ionization states are spatially coincident along the sight line so that the space densities in equation (2) can be replaced by column densities. Using the Mg radiative and dielectronic recombination rates given by Aldrovandi & Péquignot (1973)[3] and Γ(Mg I) $= (4.0 \pm 0.5) \times 10^{-11}$ cm^{-3} from Frisch et al. (1990; see also Phillips, Gondhalekar, & Blades 1981), I find the values of n_e listed in column (2) of Table 3. Adopting the dielectronic recombination parameterization for Mg I given by Shull & van Steenberg (1985) leads to a factor of {1.04, 1.39, 2.15, and 2.73} increase in the derived values of n_e at {4000, 5000, 6000, and 7000 K}. In the calculations of n_e I have neglected charge exchange processes involving Mg I since they are not well known (Péquignot & Aldrovandi 1986). Calculations of the charge exchange between Mg I and H II at high temperatures (Allan et al. 1988; see also Prasad & Huntress 1980) suggest the derived values of n_e at {5000, 6000, 8000 K} should be increased by factors of {1.46, 1.34, and 1.12}.

Unfortunately, one cannot apply equation (2) to the observations of the singly and doubly ionized atoms of Al and Si in the IVC. Recombination coefficients have been calculated for ionized Si by Aldrovandi & Péquignot (1973), but no information is available for Γ(Al II) and Γ(Si II). However, it is possible to use the strength of the fine-structure line of C II* observed toward the IVC to place additional constraints on the electron density and temperature of the gas. If collisions with electrons are the principal source of excitation of C II* in the IVC, then, following Spitzer & Fitzpatrick (1993), one can write

$$n_e(\text{cm}^{-3}) = \frac{N(\text{C II*})}{N(\text{S II})} \frac{T_e^{0.5}}{106.5} \quad (3)$$

under the assumption that C and S reside completely in the gas phase in their solar abundance ratio, which seems plausible given the abundance results presented in § 6. Lower limits on n_e imposed by the observational value of N(C II*)/N(S II) > 0.18 are given in Table 3 next to the Mg ionization balance results for several values of T_e. Including a numerical depletion $\delta = (\text{C/H})/(\text{C/H})_\odot$, of 0.33 for C decreases the numerical constant in equation (3) by a factor of 2 and increases the inferred electron density by a corresponding amount.

An additional check on the n_e-T_e space explored by the previous calculations can be made by comparing the relative abundances of Ca II and Fe II in the gas and deriving electron densities if most of the gas is neutral and a relative depletion for Ca and Fe is adopted (see Spitzer & Fitzpatrick 1993). Then the ionization balance in equation (2) can be written for Ca in terms of observable quantities

$$n_e = \frac{N(\text{Ca II})}{N(\text{Fe II})} \frac{\Gamma(\text{Ca II})}{\alpha(\text{Ca II})} \frac{N(\text{Fe})}{N(\text{Ca})}\bigg|_\odot \frac{\delta(\text{Fe})}{\delta(\text{Ca})}, \quad (4)$$

where the substitution

$$N(\text{Ca III}) \approx N(\text{Ca}) = \frac{N(\text{Ca})}{N(\text{Fe})}\bigg|_\odot \frac{\delta(\text{Ca})}{\delta(\text{Fe})} N(\text{Fe II}) \quad (5)$$

has been made. In low-density gas δ(Ca)/δ(Fe) ≈ 1 (Jenkins 1987), and the abundance results of the next section indicate that refractory element depletions are within a factor of a few of each other. Therefore, solving equation (4) subject to the constraint that δ(Ca)/δ(Fe) ≈ 0.3–1.0 should provide a reasonable estimate of the range of electron densities expected. I adopt the average value of Γ(Ca II) $= 2.0 \times 10^{-12}$ s^{-1} and calculate α_{rad}(Ca II)[4] by extrapolating the functional form given by Péquinot & Aldrovandi (1986) for $T < 1000$ K. Dielectronic recombination is not important for Ca II production at the temperatures considered here, $T < 10^4$ K (Shull & van Steenberg 1985). The n_e values derived using equation (4) are listed in column (4) of Table 3.

Two additional sources of information can be used to constrain the range of temperature in the neutral and weakly ionized IVC gas independent of the electron density. The first of these is the relative abundance of Mg I and Na I, which is highly temperature dependent above ~7000 K due to collisional ionization of Na I (Pottasch 1972). From the ionization balance represented in equation (2), one can write

$$\frac{N(\text{Mg I})}{N(\text{Na I})} = \frac{N(\text{Mg II})}{N(\text{Na II})} \frac{\Gamma(\text{Na I})}{\Gamma(\text{Mg I})} \frac{\alpha(\text{Mg I})}{\alpha(\text{Na I})} \quad (5)$$

which is independent of the electron density provided that Mg I and Na I exist in the same locations (Pettini et al. 1977; de

[3] α_{rad}(Mg I) $= 1.4 \times 10^{-13}(T_e/10^4)^{-0.855}$ cm^3 s^{-1}; α_{di}(Mg I) $= 1.7 \times 10^{-3} T_e^{-1.5} \exp(-5.1 \times 10^4/T_e)$ cm^3 s^{-1}.

[4] α_{rad}(Ca II) $= 2.8 \times 10^{-11}(T_e/10^2)^{-0.647}$ cm^3 s^{-1}; α_{di}(Ca II) $= 0$ cm^3 s^{-1} ($T_e < 10^4$ K).

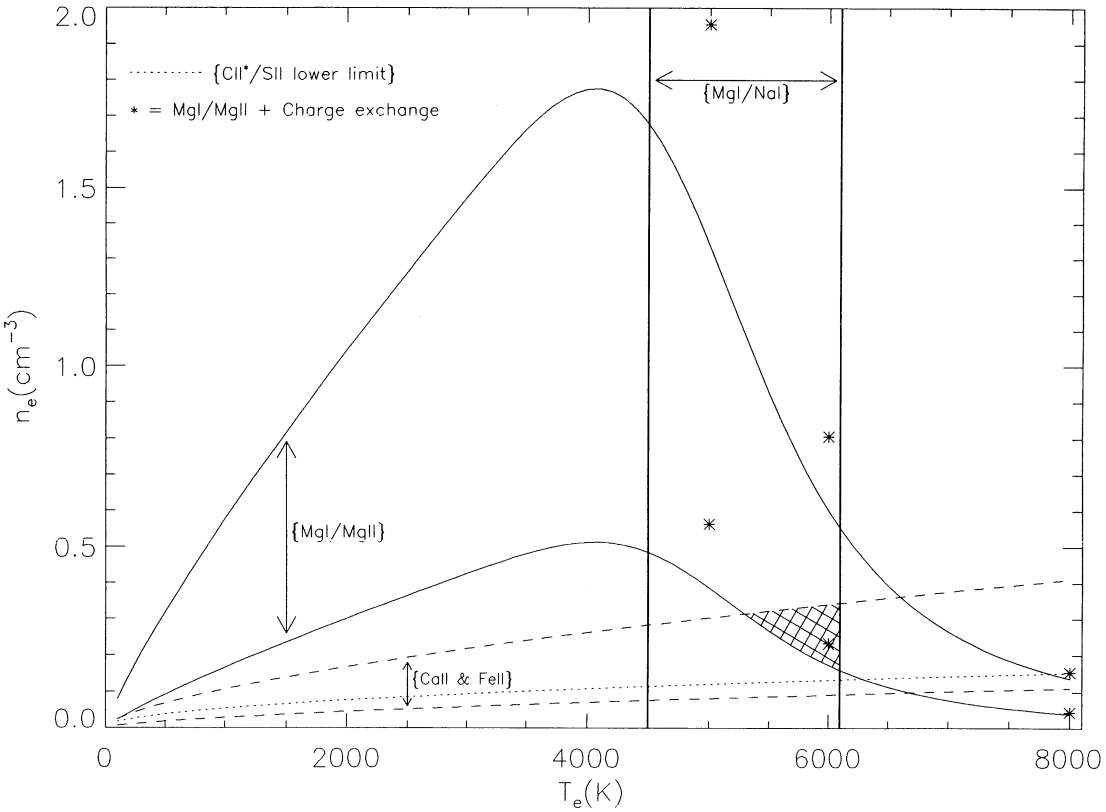

FIG. 3.—Electron density–temperature parameter space allowed by the *IUE* observations of the HD 203664 IVC absorption. The curves are labeled with the pairs of species used to determine the n_e-T_e relationships. The hatched area indicates the region that satisfies the observational constraints discussed in § 5.1 of the text. Asterisks indicate values appropriate for the Mg I–II equilibrium ionization relationship at T_e = 5000, 6000, and 8000 K if charge exchange effects with protons are included in eq. (4). See text for details.

Boer et al. 1986). Substituting

$$N(\text{Na II}) \approx N(\text{Na}) \approx \frac{N(\text{Na})}{N(\text{Mg})}\bigg|_{\odot} \frac{\delta(\text{Na})}{\delta(\text{Mg})} N(\text{Mg II}) \qquad (6)$$

into equation (5), using the average value of $\Gamma(\text{Na I}) = 1.3 \times 10^{-11}$ s^{-1}, and extrapolating the Na I radiative recombination coefficient expression[5] given by Péquinot & Aldrovandi (1986) to temperatures above 1000 K, the observed ratio of $N(\text{Mg I})/N(\text{Na I}) = 5.0$–17.5 can be satisfied for $T_e \approx$ 4500–6100 K given the value of $N(\text{Na I}) = 1.65 \times 10^{11}$ cm^{-2} found by Little et al. (1994) and the ratio $N(\text{Mg I})/N(\text{Mg II}) = (0.42\text{–}1.4) \times 10^{-2}$ found in § 4.4. In diffuse clouds, the numerical depletion of Na is at most a factor of 3 (Jura 1975; Hobbs 1976), and it is probably safe to assume $\delta(\text{Na}) \approx \delta(\text{Mg}) = 0.5$ (see § 6). Values of $N(\text{Mg I})/N(\text{Na I})$ derived using equations (4) and (5) are listed in the final column of Table 3.

The second constraint on the temperature comes from direct measurements of the widths of the H I, Na I, and Ca II lines for the main IVC absorption component at +70 km s^{-1}. This component contains most of the neutral gas associated with the IVC, and the relative *b*-values of Na I and Ca II imply a temperature $T \approx 4500$ K and turbulent velocity $V_t \approx 2.0$ km s^{-1} (Little et al. 1994). If the turbulent velocity is as low as 1.5 km s^{-1} the inferred temperature becomes $T \approx 6000$ K.

[5] $\alpha_{\text{rad}}(\text{Na I}) = 5.8 \times 10^{-12}(T_e/10^2)^{-0.682}$ cm^3 s^{-1}; $\alpha_{\text{di}}(\text{Na I}) = 0$ cm^3 s^{-1} ($T_e < 10^4$ K).

A graphical form of the results from the preceding discussion is shown in Figure 3, where n_e is plotted versus T_e. Labels identify the ionic relationship and equation used to construct each curve. The hatched region indicates the range of n_e-T_e space satisfied by the illustrated curves. These quantities are identified in boldface type in Table 3. The illustrated constraints reveal that $n_e = 0.15$–0.34 cm^{-3} and $T_e = 5300$–6100 K are allowed, as are values of $n_e \approx 0.02$ cm^{-3} near $T \approx$ 100 K.

It is unlikely that the HD 203664 IVC is a typical cool, diffuse cloud with $T \approx 100$ K. Standard cool diffuse clouds have H I column densities of $\approx 3.5 \times 10^{20}$ cm^{-3} and visual extinctions, $E(B-V)$, of ≈ 0.06 mag (Spitzer 1985). The H I column density for the HD 203664 IVC, $\sim 10^{19}$ cm^{-3} inferred from the S II measurements presented here, is more typical of warmer diffuse clouds seen along low-density sight lines through interarm regions of the Galactic disk and low halo (Sembach & Danks 1994). Diffuse clouds with temperatures near those found for the HD 203664 IVC are seen along the sight lines toward Capella ($T \approx 7000 \pm 200$ K; Linsky et al. 1993), HD 93521 ($T \approx 600$ K; Spitzer & Fitzpatrick 1993), and Sirius ($T \approx 7600 \pm 3000$ K; Lallement et al. 1994).

The electron densities in the +70 km s^{-1} IVC ($n_e \approx$ 0.15–0.34 cm^{-3}) are several times larger than the $n_e \leq 0.1$ cm^{-3} densities typically inferred for warm diffuse clouds in the aforementioned studies or the diffuse ionized gas traced by Hα emission measurements (Reynolds 1991, 1993). The uncertainties encountered in calculating the IVC n_e values tend to

favor the possibility that they may be even higher than the quoted values. Therefore, it seems reasonable to conclude that mixing between neutral and ionized gas has occurred within the IVC, although to what extent this mixing has progressed is less certain. It is not possible to ascertain a direct correspondence between the neutral and ionized gas at the resolution of these measurements, but higher resolution observations of other sight lines show elevated values of n_e when highly ionized gas species are present at velocities within a few km s^{-1} of those of the low ion lines (see, for example, Cardelli, Sembach, & Savage 1995).

5.2. *Highly Ionized Species*

The presence of Si IV and C IV at velocities near +70 km s^{-1} places strong constraints on the temperature of the highly ionized IVC gas. These species are produced primarily by collisional ionization in the interstellar medium of the Galaxy at a temperature near 10^5 K with a ratio of N(C IV)/N(Si IV) = 3.6 ± 1.3 (Sembach & Savage 1992). In the low-velocity gas toward HD 203664 N(C IV)/N(Si IV) = 3.5, and in the intermediate velocity gas N(C IV)/N(Si IV) = 4.4. For the IVC gas, the measured 2 σ upper limit of log N(N V) < 12.93 implies N(C IV)/N(N V) > 3.5, which is consistent with the Galactic average of 4.6 ± 2.6 produced in collisionally ionized gas.

Most models of collisional ionization production of the highly ionized species can reproduce the observed average value of N(C IV)/N(N V) in the Galaxy, and in some cases they can reproduce the observed N(C IV)/N(Si IV) values as well. For example, models involving mixing of hot ($T \sim 10^6$ K) and warm ($T \sim 10^4$ K) gases in the presence of turbulent flows (Slavin, Shull, & Begelman 1993) or cooling gas initially heated to a temperature near 10^6 K (Shapiro & Benjamin 1993) are capable of producing the observed ionic ratios. In the latter case, photoionization of Si IV from recombinations within the cooling gas is important but, in general, photoionization of Si IV and C IV by the ambient radiation field is not a viable production mechanism for the IVC absorption observed here because photoionization models predict very low N(C IV)/N(Si IV) ratios (see Sembach & Savage 1992 for a discussion of this topic). The relationship of lesser ionization stages to this absorption is presently unclear, but it is interesting to note that the value of N(C IV)/N(Al III) = 15.5 is very similar to the average of 14.3 ± 6.6 found by Sembach & Savage (1992).

5.3. *Future Prospects*

One must bear in mind that several potential sources of systematic errors exist in deriving the above physical conditions, including (1) adopting ionization rates appropriate for the solar neighborhood, (2) the assumption of ionization balance, (3) the assumption of spatial coincidence for various species, and (4) limited spectral resolution. The numerous assumptions needed to arrive at estimates for T_e and n_e in the IVC could be greatly reduced by higher resolution observations provided by an instrument such as the Goddard High Resolution Spectrograph (GHRS) on the *Hubble Space Telescope*. For instance, the temperature constraint provided by the N(Mg I)/N(Na I) ratio could be improved by sensitive measures of the weak Mg I lines and compared to temperature information provided through direct measurements of heavy element line widths. Measurements of n_e through equation (4) could then be used to estimate local ionization conditions [i.e., Γ(X)] at substantial distances from the Galactic plane once an accurate distance to the IVC has been determined. Higher resolution measurements would also allow one to study the velocity correspondences between low- and high-ionization gas as well as derive physical properties for individual components within the IVC rather than deriving average values as is necessary here. This final consideration could directly address the issue of whether various ions coexist within similar regions of the IVC.

6. RELATIVE ABUNDANCES IN THE IVC

6.1. *Neutral Gas*

In this section I derive the elemental depletions in the IVC under the assumption that the gas is predominantly neutral. The second ionization stage is the dominant ionic form for most of the elements of interest here (O and N being the exceptions), and depletion estimates can be made directly from the column densities listed in Table 2. The logarithmic gas phase depletion is defined using the usual notation:

$$D(\mathrm{X}) = \log \delta(\mathrm{X}) = \log \frac{\mathrm{X}}{\mathrm{S}} - \log \left.\frac{\mathrm{X}}{\mathrm{S}}\right|_{\odot}, \qquad (7)$$

where X is the element under consideration, and S is the reference element assumed to be entirely in the gas phase. For convenience, the shorthand notation X/S, which is identical to N(X)/N(S), is used when referring to a ratio of elements. In equation (7) N(S) ≈ N(S II) is the reference standard rather than N(H) ≈ N(H I)$_{21\ \mathrm{cm}}$ for the reasons described in § 4.1. Table 4 contains estimates of D(X) for C, N, O (limits only), Mg, Al, Si, Cr, Mn, Fe, and Zn. The solar abundances are from Anders & Grevesse (1989). Errors on D(X) are 1 σ estimates based upon the column density errors listed in Table 2.

Albert et al. (1993) find N(Ti II) < 1.6 × 10^{11} cm^{-2} over the +50 to +110 km s^{-1} velocity range toward HD 203664. Ti II is the dominant ion of Ti in neutral gas, and this column density implies D(Ti) < −0.74 dex. Some refractory elements

TABLE 4

HD 203664 +70 KILOMETERS PER SECOND CLOUD ABUNDANCES[a,b]

ELEMENT	$\log \left.\frac{\mathrm{X}}{\mathrm{H}}\right\|_{\odot}$	$\log \left.\frac{\mathrm{X}}{\mathrm{S}}\right\|_{\odot}$	$D(\mathrm{X}) = \log \frac{\mathrm{X}}{\mathrm{S}} - \log \left.\frac{\mathrm{X}}{\mathrm{S}}\right\|_{\odot}$	
			Neutral Gas Case	Ionized Gas Case[c]
C.....	−3.44	+1.29	> −1.44	> −1.50
N	−3.95	+0.78	> −1.40	> −0.76
O	−3.07	+1.66	> −1.70	> −1.12
Mg[d].....	−4.41	+0.32	$-0.30^{+0.08}_{-0.10}$	−0.16
Al	−5.52	−0.79	> −0.66	> −0.25
Si	−4.45	+0.28	$-0.43^{+0.09}_{-0.11}$	−0.40
Ti[e]	−7.07	−2.34	< −0.79	...
Cr.....	−6.32	−1.59	$-0.31^{+0.13}_{-0.18}$	*+0.03*
Mn	−6.47	−1.74	$-0.40^{+0.19}_{-0.35}$	*−0.06*
Fe.....	−4.49	+0.24	$-0.57^{+0.09}_{-0.11}$	−0.23
Zn	−7.35	−2.62	$+0.28^{+0.19}_{-0.34}$	*+0.62*

[a] Solar abundances are from Anders & Grevesse 1989.

[b] $\log (\mathrm{S/H})|_{\odot} = -4.73$.

[c] Values for elements in italics represent estimates made by scaling the neutral gas depletions by the DIG ionization correction appropriate for Fe II (see § 6.2).

[d] Only Mg II is considered in the neutral gas depletion estimate. Including Mg I increases D(Mg) by <0.01 dex.

[e] Neutral gas depletion estimate of Ti based upon the value of log N(Ti II) < 11.20 measured by Albert et al. 1993.

may therefore have depletions more severe than that of Fe by a factor of 1.5 or more. This result is consistent with the earlier contention in § 5 that $\delta(\mathrm{Ca})/\delta(\mathrm{Fe}) < 1.0$ since Ca is usually at least as depleted from the gas phase as Ti (Jenkins 1987).

6.2. *Partially Ionized Gas*

The ions used to deduce the gas phase depletions in § 6.1 may also exist in partially ionized gas (i.e., in H II regions). There are several reasons to believe that ionized gas contributions may affect the depletion estimates derived in § 6.1:

1. The presence of doubly and triply ionized gas species (e.g., Al III, Si III, Si IV, C IV) at velocities indistinguishable from those of the lower ionization species.
2. The discrepancy in the H I column densities measured from the 21 cm emission profile shown in Figure 1 and deduced from the S II absorption measurements under the assumption that S II traces only neutral gas in the IVC.
3. The large electron densities ($n_e \approx 0.15$–0.34 cm^{-3}) derived in § 5.
4. The differences in the COG b-values derived for O I and N I (<5.0 km s^{-1}; see § 4), which reside primarily in H I regions, compared to those derived for the singly ionized metals having ionization potentials spanning the 13.6 eV energy range (8–12 km s^{-1}).

While none of these reasons alone is sufficient to claim that $N(\mathrm{H\ II}) > N(\mathrm{H\ I})$, taken together they provide a powerful incentive to more fully explore the effects of ionization on the depletions derived under the assumption that the gas is completely neutral.

To explore the effects of ionization on the depletions derived previously, I use the results of a model for the ionization of a diffuse ionized gas (DIG). The DIG results have been kindly provided by John Mathis and reflect a set of conditions appropriate for the situation in which $N(\mathrm{S\ II})/N(\mathrm{H\ I})_{21\ \mathrm{cm}} \approx N(\mathrm{S\ II})/N(\mathrm{H\ I})_{\mathrm{model}}$. This requirement is equivalent to satisfying reason (2) for believing ionized gas contributes to the measured S II column density. The model results predict $N(\mathrm{Al\ II}):N(\mathrm{Al\ III}) = 1.9{:}1.0$ and $N(\mathrm{Si\ II}):N(\mathrm{Si\ III}):N(\mathrm{Si\ IV}) = 2.5{:}1.0{:}0.13$, in general agreement with the limits imposed by the observations. The model is based upon an H II region model for Kurucz 36675 and can justifiably be considered a limiting case to the hardness of the radiation field since higher ionization parameter models fail to satisfy the observational constraints. Information about various DIG ionization models can be found in Dömgorgen & Mathis (1994).

Assuming most of the IVC gas occurs in the dilute H II region, one can write

$$n(\mathrm{X}^+) = n(\mathrm{X})k(\mathrm{X}^+) \tag{8}$$

where $k(\mathrm{X}^+)$ is the ionization fraction of the singly ionized atom. Then equation (7) becomes

$$D(\mathrm{X}) = \log\left[\frac{\mathrm{X}}{\mathrm{S}}\frac{k(\mathrm{S}^+)}{k(\mathrm{X}^+)}\right] - \log\left.\frac{\mathrm{X}}{\mathrm{S}}\right|_{\odot}. \tag{9}$$

The fifth column of Table 4 lists the gas phase depletions for the IVC derived by scaling the values in column (4) by the appropriate ionization fractions of S II and the remaining ions in the ionized gas. In all but one case (C II), the inferred values of $D(\mathrm{X})$ increase (i.e., the depletion is less severe) than for the case in which the gas is assumed to be completely neutral. This occurs because we are referencing the abundances with respect to S II rather than H I. The ionization fraction of S II is greater than it is for the other observed ions; the second ionization potential of sulfur ($\chi_{\mathrm{II}} = 23.3$ eV) is larger than it is for the other singly ionized species ($\chi_{\mathrm{II}} \approx 15$–$17$ eV) and therefore $k(\mathrm{S}^+) \geq k(\mathrm{X}^+)$.

For elements not explicitly incorporated into the diffuse ionized gas calculations (Cr, Mn, Zn), the model ionization fraction results have been scaled to those for Fe to produce depletion estimates for these elements for the partially ionized gas case. These values are indicated in italics in Table 4 and should be considered approximations only.

7. DISCUSSION

The results of the preceding sections indicate that the relative abundances of the elements in the HD 203664 IVC are within a factor of 5 of solar values, which means that either material within the IVC has undergone enough processing to liberate most of the elements locked into dust back into the gas or the IVC contained little dust originally. The detection of highly ionized gas species usually attributed to shocks (e.g., Si IV and C IV) suggests that the former of these two possibilities is the more likely. To produce observable amounts of Si IV and C IV by collisional ionization requires shocks with $v_{\mathrm{sh}} \approx 100$–$120$ km s^{-1} (see, for example, Raymond, Wallerstein, & Balick 1991). Grain destruction by nonthermal sputtering and grain-grain collisions is usually severe in gas behind shocks with these speeds; in fact, shock speeds as low as 40 km s^{-1} are sufficient to reproduce the approximate ratios of Si, S, and Fe found for the IVC (see Seab & Shull 1983). The $N(\mathrm{Ca\ II})/N(\mathrm{Na\ I})$ ratio of ≈ 3 derived by Little et al. (1994) for the absorption in the IVC is typical of peculiar gas velocities in excess of 50 km s^{-1} (see Sembach & Danks 1994).

Gas in the IVC has a peculiar velocity relative to gas participating in Galactic rotation in this direction. At the distance of HD 203664, corotating gas has an LSR velocity of $+27$ km s^{-1}, which indicates that the IVC gas has a peculiar velocity of ≥ 40 km s^{-1}. The velocity limits of the absorption defined in § 3 imply that much of the gas may have peculiar velocities as large as about 90 km s^{-1} if the gas is located within a few hundred parsecs of the Sun. The velocity limits and depletion estimates are consistent with the observation that IVCs and HVCs tend to have substantially lower dust contents than low velocity gas clouds (Wakker & Boulanger 1986) and suggest that the total peculiar velocity of the cloud may be considerably higher than the radial component indicates.

The gas phase abundances inferred for the HD 203664 IVC are more akin to those of the warm intercloud environments than cool, diffuse cloud environments (Jenkins et al. 1986), which is consistent with the temperature $T \approx 6000$ K found in § 5. The very low heavy element depletions are typical of those seen in shocked gas in SNRs and other extreme environments, and although Al III is usually not detected in SNRs, the relative abundances of Si IV, C IV, and N V in the IVC are in agreement with those seen toward young SNRs like Vela (Jenkins, Wallerstein, & Silk 1984). Bates et al. (1983) ruled out the main ridge of Radio Loop II gas as an origin for the IVC on the basis of the IVC velocity and available observational parameters for the loop but could not exclude the possibility that smaller features within Loop II may give rise to the IVC absorption.

The highly ionized gas associated with the IVC is probably located at the boundary of the cloud between a hotter surrounding medium and the warm gas of the IVC. Using the high-resolution echelle mode of the GHRS to observe HD

167756, a low-latitude halo star at $z \approx -800$ pc, Savage, Sembach, & Cardelli (1994) found structured low-ionization absorption components with C IV to S IV ratios similar to those of the HD 203664 IVC. They attributed this absorption to conductive interfaces of the type described by Borkowski, Balbus, & Fristrom (1990). It is possible that the HD 203664 IVC is a condensation or accelerated cloud in a hot ($T \sim 10^6$ K) cooling flow due to supernova explosions in the disk that result in "chimneys" (Norman & Ikeuchi 1989) or "fountains" (Shapiro & Field 1976; Bregman 1980) of hot gas expelled into the low halo.

To summarize, it appears that the IVC toward HD 203664 is composed of a warm ($T \approx 6000$ K) diffuse cloud(s) which is neutral or partially ionized and has a highly ionized boundary resulting from collisional ionization at high temperatures ($T \sim 10^5$ K). The relative abundances of heavy elements in the IVC are within a factor of 5 of their solar values, which suggests that dust grains in the IVC have been heavily processed, perhaps by the same processes (shocks, etc.) producing the highly ionized species. The origin of the cloud is uncertain, but a scenario involving heated gas escaping from the disk into the halo appears to be consistent with a present z-distance of several hundred parsecs or more for the IVC and an initial chemical enrichment characteristic of Population I stars in the Galactic disk. The high-resolution optical data for this sight line suggest a multiple component structure for the IVC, and therefore higher resolution ultraviolet observations could help to provide further insight into the physical conditions and structure within various portions of the IVC.

It is a pleasure to thank Francis Keenan and Philip Dufton for encouragement and discussion about the HD 203664 sight line and for providing the 21 cm profile shown in Figure 1. I also thank John Mathis for making his DIG model results available to me in advance of publication and for useful discussion of H II region abundances and ionization issues. I am grateful to the *IUE* staff for their assistance with the remote observations and data processing aspects of the project. Support for this work was provided by a Hubble Fellowship through grant HF-1038.01-92A from the Space Telescope Science Institute, which is operated by AURA under NASA contract NAS 5-26555.

REFERENCES

Albert, C. E., Blades, J. C., Morton, D. C., Lockman, F. J., Proulx, M., & Ferrarese, L. 1993, ApJS, 88, 81
Aldrovandi, S. M. V., & Péquignot, D. 1973, A&A, 25, 137
Allan, R. J., Clegg, R. E. S., Dickinson, A. S., & Flower, D. R. 1988, MNRAS, 235, 1245
Anders, E., & Grevesse, N. 1989, Geochim. Cosmochim. Acta, 53, 197
Bates, B., Brown-Kerr, W., Giaretta, D. L., & Keenan, F. P. 1983, A&A, 122, 64
Berkuijsen, E. M., Haslam, C. G. T., & Salter, C. J. 1971, A&A, 14, 252
Borkowski, K. J., Balbus, S. A., & Fristrom, C. C. 1990, ApJ, 355, 501
Bowen, D., & Blades, J. C. 1993, ApJ, 403, L55
Bregman, J. N. 1980, ApJ, 236, 577
Cardelli, J. A., Sembach, K. R., & Savage, B. D. 1995, ApJ, 440, 241
Cardelli, J. A., Sofia, U. J., Savage, B. D., Keenan, F. P., & Dufton, P. L. 1994, ApJ, 420, L33
Danly, L. 1989, ApJ, 342, 785
Danly, L., Albert, C. E., & Kuntz, K. D. 1993, ApJ, 416, L29
Danly, L., Lockman, F. J., Meade, M. R., & Savage, B. D. 1992, ApJS, 81, 125
de Boer, K. S., Lenhart, H., van der Hucht, K. A., Kamperman, T. M., Kondo, Y., & Bruhweiler, F. C. 1986, A&A, 157, 119
Diplas, A., & Sembach, K. R. 1995, in preparation
Dömgorgen, H., & Mathis, J. S. 1994, ApJ, 428, 647
Dufton, P. L., Hibbert, A., Kingston, A. E., & Tully, J. A. 1983, MNRAS, 202, 145
Dufton, P. L., Keenan, F. P., Hibbert, A., Ojha, P. C., & Stafford, R. P. 1992, ApJ, 387, 414
Frisch, P. C., Welty, D. E., York, D. G., & Fowler, J. R. 1990, ApJ, 357, 514
Hobbs, L. M. 1976, ApJ, 203, 143
Hulsbosch, A. N. M., & Wakker, B. P. 1988, A&AS, 75, 191
Jenkins, E. B. 1986, ApJ, 304, 739
———. 1987, in Interstellar Processes, ed. D. Hollenbach & H. A. Thronson (Dordrecht: Reidel), 533
Jenkins, E. B., Savage, B. D., & Spitzer, L. 1986, ApJ, 301, 355
Jenkins, E. B., Wallerstein, G., & Silk, J. 1984, ApJ, 278, 649
Jura, M. 1975, ApJ, 200, 415
Keenan, F. P., Dufton, P. L., McKeith, C. D., & Blades, J. C. 1983, MNRAS, 203, 963
Lallement, R., Bertin, P., Ferlet, R., Vidal-Madjar, A., & Bertaux, J. L. 1994, A&A, 286, 898
Lennon, D. J., Dufton, P. L., Keenan, F. P., & Holmgren, D. E. 1991, A&A, 246, 175
Linsky, J. L., et al. 1993, ApJ, 402, 694
Little, J. E., Dufton, P. L., Keenan, F. P., & Conlon, E. S. 1994, ApJ, 427, 267
Lu, L., Savage, B. D., & Sembach, K. R. 1994, ApJ, 426. 563
Morton, D. C. 1991, ApJS, 77, 119
Nachman, P., & Hobbs, L. M. 1973, ApJ, 273, 450
Norman, C., & Ikeuchi, S. 1989, ApJ, 345, 372
Pettini, M., Boksenberg, A., Bates, B., McCaughan, R. F., & McKeith, C. D. 1977, A&A, 61, 839
Péquignot, D., & Aldrovandi, S. M. V. 1986, A&A, 161, 169
Phillips, A. P., Gondhalekar, P. M., & Blades, J. C. 1981, MNRAS, 195, 485
Pottasch, S. R. 1972, A&A, 20, 245
Prasad, S. S., & Huntress, W. T. 1980, ApJS, 43, 1
Raymond, J. C., Wallerstein, G., & Balick, B. 1991, ApJ, 383, 226
Reynolds, R. J. 1991, ApJ, 372, L17
———. 1993, in Back to the Galaxy, ed. S. Holt & F. Verter (New York: AIP), 156
Savage, B. D., et al. 1993a, ApJ, 413, 116
Savage, B. D., Lu, L., Weymann, R., Morris, S., & Gilliland, R. 1993b, ApJ, 404, 124
Savage, B. D., & Sembach, K. R. 1991, ApJ, 379, 245
———. 1994, ApJ, 434, 135
Savage, B. D., Sembach, K. R., & Cardelli, J. 1994, ApJ, 420, 183
Savage, B. D., Sembach, K. R., & Lu, L. 1995, ApJ, in press
Seab, C. G., & Shull, J. M. 1983, ApJ, 275, 652
Sembach, K. R., & Danks, A. C. 1994, A&A, 289, 539
Sembach, K. R., & Savage, B. D. 1992, ApJS, 83, 147
Sembach, K. R., Savage, B. D., & Lu, L. 1995, ApJ, 439, 672
Shapiro, P. R., & Benjamin, R. A. 1993, in Star Forming Galaxies and Their Interstellar Media, ed. J. J. Franco (New York: Cambridge Univ. Press), 273
Shapiro, P. R., & Field, G. B. 1976, ApJ, 205, 762
Shull, J. M., & van Steenberg, M. 1985, ApJS, 48, 95
Slavin, J. D., Shull, J. M., & Begelman, M. C. 1993, ApJ, 407, 83
Spitzer, L., Jr. 1985, ApJ, 290, L21
Spitzer, L., Jr., & Fitzpatrick, E. 1993, ApJ, 409, 299
Sutherland, R. S., & Dopita, M. A. 1993, ApJS, 88, 253
Wakker, B. P., & Boulanger, F. 1986, A&A, 170, 84
Wakker, B. P., & Schwarz, U. J. 1991, A&A, 250, 484
Wakker, B. P., & van Woerden, H. 1991, A&A, 250, 509